Full Paper

Propellants, Explosives, Pyrotechnics

DOI: 10.1002/prep.201600097

Quantitative Schlieren Measurement of Explosively-Driven Shock Wave Density, Temperature, and Pressure Profiles

Jesse D. Tobin[a] and Michael J. Hargather*[a]

Abstract: Shock waves produced from the detonation of laboratory-scale explosive charges are characterized using high-speed, quantitative schlieren imaging. This imaging allows the refractive index gradient field to be measured and converted to a density field using an Abel deconvolution. The density field is used in conjunction with simultaneous piezoelectric pressure measurements to determine the shock wave temperature decay profile. Alternatively, the shock wave pressure decay profile can be estimated by assuming the shape of the temperature decay. Results are presented for two explosive sources. The results demonstrate the ability to measure both temperature and pressure decay profiles optically for spherical shock waves that have detached from the driving explosion product gases.

Keywords: Schlieren · Explosive temperature · Quantitative optical techniques

1 Introduction

Characterization of explosive effects has traditionally been performed using pressure gages and various measures of damage, such as plate dents, to determine a "TNT Equivalence" of a blast [1,2]. Most of the traditional methods, however, result in numerous equivalencies for the same material due to large uncertainties and dependencies of the equivalence on the distance from the explosion [3,4]. Modern high-speed digital imaging has allowed the development of several optical techniques for studying explosive effects, which have expanded the detail to which a blast can be characterized.

Many of the imaging studies visualize and track shock wave propagation using refractive imaging techniques including schlieren, shadowgraphy, and background oriented schlieren (BOS) [5]. In one of the most ground-breaking studies, Kleine et al. used high-speed digital cameras and shadowgraphy to track shock waves from silver azide charges and demonstrated the spatial dependence of a "TNT equivalence" measurement [6]. Similar studies expanded the analysis using other imaging methods [7,8], explosive materials [9–12], and explosive-charge scales [13–15]. All of these approaches have focused on measuring the shock wave propagation optically to estimate pressure characteristics which are compared to gage measurements.

The schlieren and BOS technique are capable of yielding quantitative density information of flow fields [16], but few researchers have applied this capability to studying explosions. Quantitative density measurement from refractive techniques is well-documented for aerodynamics applications [17–19], including shock waves [20], but not moving shocks. One exception is the technical report by Biss and McNesby [21], where quantitative schlieren imaging was used to measure the density field near a small explosive charge. This work used the quantitative density measurement to estimate the pressure field and impulse produced by the explosion as a function of distance. The pressure measurement, however, relied on an assumed temperature.

The measurement of temperature in explosive events can be considered a "holy grail", which many researchers have explored [22–24]. The challenges include temporal and spatial resolutions across orders of magnitude temperature changes, as well as the destructive environment of the explosion itself. One of the most successful techniques has been optical pyrometry and spectroscopy [25,26]. These techniques measure a temperature in a limited region of an explosive fireball, but do not provide any information on the temperature associated with the shock wave, which in general propagates further than the fireball.

The present work applies schlieren diagnostics to quantitatively measure the density field produced by an explosively-driven shock wave, as done by Biss [21]. We expand on the previous work by using piezoelectric pressure gages to measure the simultaneous pressure field behind the shock wave. From these two measurements the temperature decay behind the moving shock wave is determined. Scaling arguments are applied using the measured data and computational simulations to allow estimation of the temperature and ultimately pressure field from just the optically-measured density field.

[a] *J. D. Tobin, M. J. Hargather*
Mechanical Engineering Department, New Mexico Tech, 801 Leroy Place, Socorro, NM 87801, USA
**e-mail: michael.hargather@nmt.edu*

2 Experimental Section

2.1 Schlieren Imaging Setup

A parallel-light lens schlieren system [5] was used as shown schematically in Figure 1. The system includes two 127 mm diameter f/6 parabolic lenses, an LED light source, and a razor blade knife edge. Images were captured with a high-speed digital camera, for which both a Photron SA-X2 and a Phantom v711 were used in individual experiments. The choice of camera did not affect the results and represents a user preference.

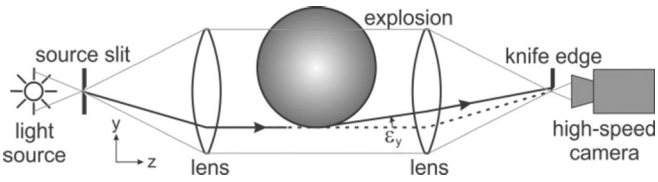

Figure 1. Schematic of a parallel-light lens schlieren system, showing a ray of light being refracted by a shock wave in the test section. The coordinate system shown uses *z* along the optical axis and *x* and *y* perpendicular to the optical axis, with *y* in the vertical direction shown.

The schlieren technique visualizes the derivative of the refractive index field integrated along the optical path [5]. The region between the parabolic lenses is considered the "test section", and the refractive index variations throughout this region are imaged. The quantitative density measurement process is well documented by Hargather and Settles [16] and only a limited description of the process is reproduced herein.

A schlieren image is characterized by grayscale pixel intensity variations representing the refractive index gradient field. To quantify the variations, a calibration object is used to relate grayscale intensity to refraction angle (gradient of refractive index) [16]. Here 4 m and 10 m focal length lenses were used as the calibration objects. The grayscale variations across the lenses are directly correlated to the grayscale values in the flow region of interest to determine the local refraction angle. Figure 2 shows the grayscale variation across a typical schlieren image with the calibration lens and a shock wave in the field of view. Typically separate tests are performed, one to record images of the calibration lens and then the actual explosive test without the lens in the field of view. Experiments showed that as long as the optical system was not adjusted or moved between tests, the calibration data could be used from the separate test, thus allowing the field of view to be free of the lens. The calibration lens is positioned in the plane of the shock wave to be measured, and the camera is focused on the lens.

The grayscale variation as a function of position within the lens is fit to a linear profile. Each radial position in a lens focuses light toward the lens focal point, thus each radial position has a different angle through which light is bent. The grayscale gradient across the lens is thus related to refraction angle for known lens focal length. The lens in Figure 2 has only a horizontal variation in intensity, instead of a polar angle variation, because a vertical knife edge [5] is used in the schlieren imaging yielding visualization of only horizontal refractions.

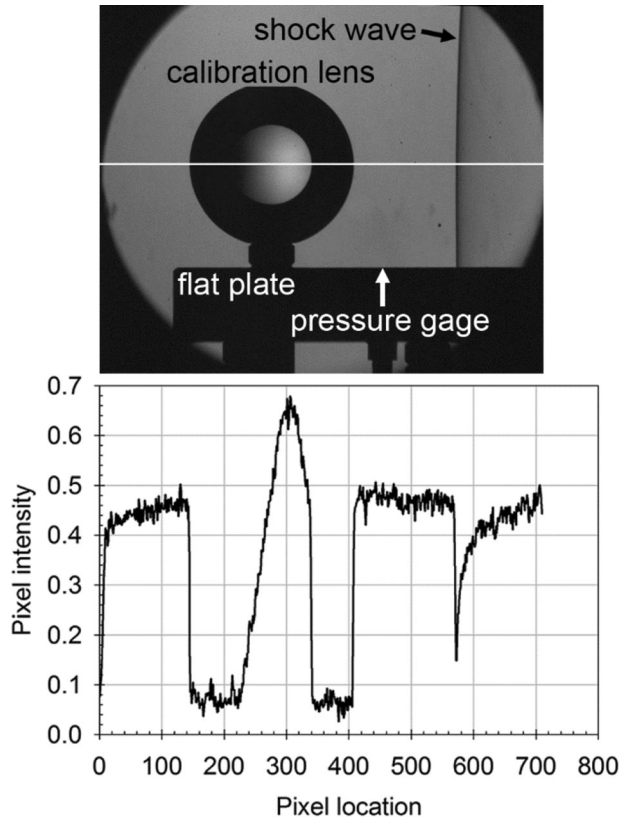

Figure 2. Typical full-field schlieren image showing the calibration lens and a shock wave propagating to the left. The graph shows the pixel intensity along the horizontal white line in the image. The outer diameter of the lens holder is 45 mm.

The refraction angle, ε_y, is the angle through which a light ray has been bent and is given by:

$$\varepsilon_y = \frac{1}{n}\int \frac{dn}{dy} dz \tag{1}$$

The integral yields the total light bending along the entire optical path. For a rectilinear two-dimensional flow the refractive index gradient field is assumed to be independent of length along the optical axis (*z* in Figure 1), and the integral yields the gradient multiplied by depth of the refracting object. For the spherical geometry of an expanding shock wave, the integral is not as easily simplified: an Abel transform is required.

DOI: 10.1002/prep.201600097

2.2 Abel Transformation

The Abel transformation relates a spherically-symmetric field to a two-dimensional projection of the field [27] and is used herein to deconvolute the planar schlieren projection to the radially-symmetric three-dimensional refractive index field [28]. The two-point method described by Kolhe and Agrawal [28] is used.

The Abel transformation has an input of the refraction angle in radians at each radial point in the image, ε_j, and the output is $\delta(r_i)$, which as shown below is a non-dimensionalized refractive index, n, value at each corresponding radial position, r_i. The Abel transformation is performed by solving the following equations:

$$\delta(r_i) = \sum_{j=i}^{N+1} D_{i,j} \cdot \varepsilon_j \tag{2}$$

$$D_{i,j} = \begin{cases} \frac{1}{\pi}\left(A_{i,j} - A_{i,j-1} - jB_{i,j} + (j-2)B_{i,j-1}\right), \\ \qquad \text{if } j > i \text{ and } j \neq 2 \\ \frac{1}{\pi}\left(A_{i,j} - jB_{i,j} - 1\right), \text{if } j > i \text{ and } j = 2 \\ \frac{1}{\pi}\left(A_{i,j} - jB_{i,j}\right), \text{if } j = i \text{ and } i \neq 1 \\ 0, \text{if } j = i = 1 \text{ or } j < i \end{cases} \tag{3}$$

$$A_{i,j} = \sqrt{j^2 - (i-1)^2} - \sqrt{(j-1)^2 - (i-1)^2} \tag{4}$$

$$B_{i,j} = \ln\left(\frac{j + \sqrt{j^2 - (i-1)^2}}{(j-1) + \sqrt{(j-1)^2 - (i-1)^2}}\right) \tag{5}$$

$$\delta(r_i) = \frac{n(r_i)}{n_0} - 1 \tag{6}$$

The local refraction angle, ε_j, is obtained from the image using the local intensity value and the calibration lens to convert that intensity to a refraction angle. The Abel transform requires the refraction field from the radial point being analysed all of the way to the center of the spherical object. For tests performed herein, where the center of the shock wave is not visible, the pixel locations from the edge of the field of view to the center are filled with values of 0. This does not affect the determination of the local refractive index, but is required for the Abel inversion process.

The Abel inversion assumes and requires that the entire field being inverted is of the same material. This technique can be applied across the shock wave in air, but cannot be applied in areas where the gas changes, e.g. from the air to the product gas cloud. This limits the analysis here to shock waves which have separated from the driving product gases.

Once obtained, the refractive index, n, of the gas can be directly related to density, ρ, by the Gladstone-Dale Law using the Gladstone-Dale constant for air ($k = 2.23 \times 10^{-4}\ \mathrm{m^3\,kg^{-1}}$):

$$n = k\rho + 1 \tag{7}$$

2.3 Pressure Measurement

Side-on pressure was measured for each test using a PCB Piezotronics model 102A07 gage, with maximum pressure of 345 kPa (50 psi). The pressure gage was flush-mounted in an aluminum flat plate, which was rigidly mounted to an optical table. The plate was positioned with the top surface parallel to the explosion center. The sharp leading of the plate was pointed at the blast center, resulting in the shock wave propagating across the plate, while remaining effectively perpendicular to the plate. Experiments showed good alignment of the plate and explosion center, with no Mach stems or irregular reflections observed.

The flat plate and pressure gage were positioned in the schlieren system test section with the plate top surface located just below the centerline of the imaging. Figure 2 shows the full schlieren field of view, with the rear portion of the flat plate visible. The location of the flush-mounted pressure gage is noted in the image. Atmospheric pressure during testing was measured with a laboratory weather station and verified against the nearby Socorro, NM, airport weather reporting.

2.4 Blast Wave Property Variations

The goal of this work was to measure temperature and pressure variation across an explosively-driven shock wave. Before experiments were performed the analytical solution of Taylor [29] was explored to provide a theoretical variation of properties. The blast wave similarity solution as developed by Taylor shows that the density and pressure both vary over the same time scale. The decay profiles are plotted together as the non-dimensional pressure and density as functions of radius from the explosion center in Figure 1 of Ref. [29].

To further support this assumption that the pressure and density can be assumed to vary over the same timescale, simple computational simulations were performed in CTH. CTH is a hydrocode developed by Sandia National Laboratories and is used widely to examine shock physics and shock wave propagation from explosions [30]. Herein a simple one-dimensional radially symmetric computation was performed. The explosion of a 1 g charge of PETN was simulated in a domain with a 2 m radial extent. The domain was divided into 2000 individual cells, providing a base resolution of 1 mm. Computational gages were positioned every 10 mm to obtain density, temperature, and pressure profiles as a function of time at individual locations. The output here is not of interest in absolute magnitude, but rather a scaled magnitude to examine the timescale of property changes. The field variables of tempera-

ture, pressure, and density were normalized by the maximum calculated value behind the shock wave and the atmospheric values as:

$$T^* = \frac{T - T_{atm}}{T_{max} - T_{atm}} \quad (8)$$

With this normalization the peak values become a 1, atmospheric values will be 0, and values below atmospheric conditions will be negative. The non-dimensional results of the simulation at a distance of 0.9 m from the explosion are shown in Figure 3. The results show that the density, pressure, and temperature all vary over the same timescale, as predicted by the Taylor similarity solution. This assumption is used here to estimate the time of the return to atmospheric pressure and temperature from the measured optical density data, as discussed below.

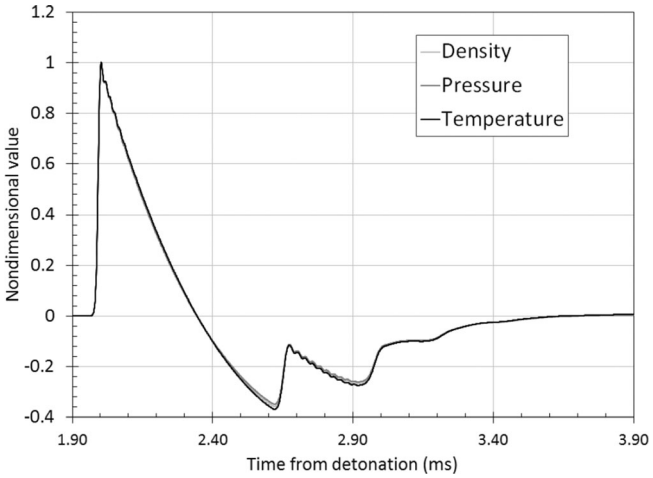

Figure 3. Non-dimensionalized density, pressure, and temperature profiles at a location 0.9 m from a 1 g PETN detonation simulated with CTH.

2.5 Experimental Procedure

Experiments were performed using shotgun primers (Remington 209 Premier STS) and 1 g spheres of primasheet (Ensign-Bickford, 80% PETN). Additional experiments were performed using NONEL shock-tube (Dyno Nobel), but are not presented here because the results were similar to the primers and primasheet [31].

For each test the explosive was positioned at a known distance from the schlieren field of view and pressure gage location. The explosive center was positioned in line with the pressure measurement plate top surface. Each explosive was suspended so that no reflections from the optical table (ground reflections) interferred with the measurements.

The schlieren system was set up so that the background intensity variation (grayscale level in Figure 2) was as uniform as possible. The background had a typical standard deviation of about 30 intensity levels, for the 12-bit cameras used, or about 0.7%.

A high-speed digital camera was used to record the schlieren images. The frame rates varied between tests, but were generally greater than 100,000 frames per second (except for full-field images, which were recorded for visualization purposes but not used for the primary data). The shutter speed was generally set to the minimum possible shutter speed of 0.293 μs or 0.30 μs for the Photron and Phantom cameras, respectively.

The schlieren system light source illumination and cutoff fraction were adjusted to maximize the range of grayscale intensity levels in the images. The number of pixel intensity values used (dynamic range) directly relates to the sensitivity of the system, or the smallest refraction angle that can be resolved. By maximizing the dynamic range in the images, finer the resolution of the density reconstruction can be achieved. Image processing including histogram stretching and gamma corrections [32] are not performed on the images before performing the density measurement, as no additional information is gained from the image processing. Most of the images presented here are raw, unadjusted, but some have been histogram-stretched to enhance visibility of flow features for publication.

An image of the calibration lens was recorded with the high-speed camera before and after each test. The calibration lens was used to relate the pixel grayscale intensity to a quantitative refraction angle, ε_j. Once this image was recorded, the camera and schlieren system were not adjusted before performing a test.

Each explosive test recorded high-speed images of the shock wave propagation over the flat plate and the pressure-time history from the piezoelectric pressure gage. The image data was analysed with the Abel transformation to obtain the refractive index and density fields. The pressure-time data and density field data were then analysed to determine temperature fields and an optical estimate of pressure throughout the blast field.

3 Results and Discussion

The results discussed are from a sequence of experiments performed over several months at the Energetic Materials Research and Testing Center (EMRTC), a research division of New Mexico Institute of Mining and Technology, located adjacent to campus in Socorro, NM.

Experiments were performed to image the shock wave from shotgun primers and 1 g spheres of primasheet. The shotgun primers were fired from a manual, spring-loaded, commercially-available device. The primers were positioned 0.165 m from the pressure gage location. This distance allowed the shock wave to separate sufficiently from the driving combustion gases. The shotgun primer face was pointed at roughly a 45 degree angle upward. Small frag-

DOI: 10.1002/prep.201600097

ments were expelled from the primer during firing, so this orientation reduced the fragments in the images and the associated noise in the pressure and density measurements.

Primasheet spheres were positioned 0.902 m from the pressure gage. The spheres were rolled by hand from the sheet explosive and were as round as possible. The detonator was positioned downward into the spheres which were suspended in air.

3.1 Schlieren Imaging and Density Measurement

The high-speed cameras recorded schlieren images of the shock wave propagation throughout the field of view. A typical image sequence of the shock wave is shown in Figure 4. The sequence was recorded at 120,000 frames per second, yielding the long rectangular frame size, which is ideal for imaging the one-dimensional shock wave motion over the flat plate. The pressure gage is flush-mounted in the flat plate at the position just behind the shock wave leading edge in Figure 4d.

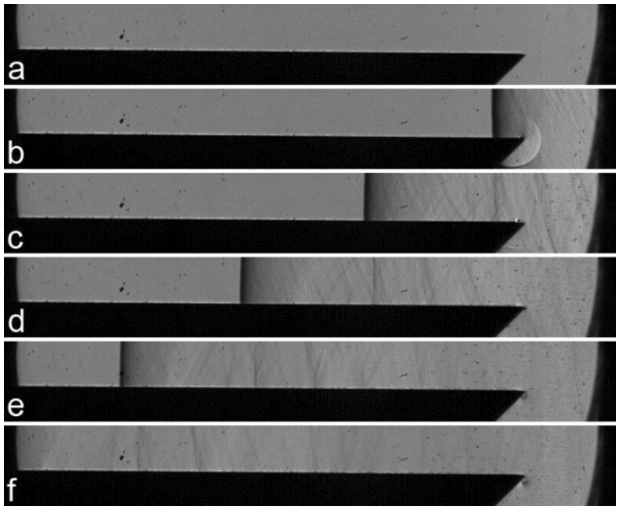

Figure 4. Typical schlieren image sequence showing the shock propagating from right to left over the flat plate. The shock wave is just to the left of the pressure gage in image d. The image in frame a is set a $t = 0$ for all analysis and subsequent images shown are 67 microseconds apart.

3.1.1 Digital Streak Images

The individual high-speed images are used to create a digital streak image, which is shown in Figure 5. This streak image is created by extracting one pixel row from each image and stacking these rows vertically for successive images. The final streak image thus shows horizontal position on the horizontal axis and time on the vertical axis, with time increasing downward in the image. The streak image is used to measure the shock wave position as a function of time and velocity as it moves through the test region.

The streak image illustrates a unique transformation that needed to be performed on the recorded data to directly relate the density field to the time-resolved pressure field. The pressure gage measures the static pressure at a single location as a function of time, whereas the high-speed camera images density across a spatial field at individual times (individual frames). In order to compare the measured optical density to the measured pressure the coordinate reference frame of one of these two data sets must be transformed. To agree with traditional explosive measurements, the density field is converted to density as a function of time at the pressure gage location. This transformation is effectively converting from a horizontal line in the streak image to a vertical line. The temporal resolution of the high-speed camera was lower than the spatial resolution, so taking a vertical column from the streak image (Figure 5b) was not ideal. Instead the time-resolved density field was created by transforming the spatial density field (Figure 5c) using the velocity of the shock wave propagation. The streak image shows that the shock wave is not significantly varying in speed over the imaged area (constant slope in the streak image), so the errors are expected to be small from this manipulation. The transformed pixel intensity field is shown in Figure 5d, plotted with the time-resolved intensity extracted from the vertical line in the streak image. The two intensity curves agree well, as expected, but the transformed data set is of significantly higher temporal resolution.

3.1.2 Density Measurement from Abel Transform

The density field is obtained by performing an Abel transform on the measured camera intensity data. The measured intensity at each pixel is first converted to a local refraction angle using the calibration lens [16].

The physical distance from the center of the explosive charge to each pixel is determined using a pixel-to-length calibration and a physical measurement from the pressure gage to the explosive center.

The data for local refraction angle, ε_j, at each physical location, r_i, are the two inputs to the Abel transform (Equation (2), Equation (3), Equation (4), Equation (5), and Equation (6)), which outputs the refractive index as a function of radial position n_i. The radial information is transformed to a temporal density field.

The intensity data in Figure 5c was extracted from the image in Figure 4d, and is transformed to the density profile shown in Figure 6, presented with the original intensity variation for reference. The data shown was calculated using a single row of pixels extracted from the image in Figure 4d. The analysis was repeated with an input of pixel intensity at each location averaged over three rows of pixels, for which the results were indistinguishable on the graph. The averaging was explored to reduce sensor-level noise in the pixel intensities recorded, but the Abel transform process makes these small variations insignificant in

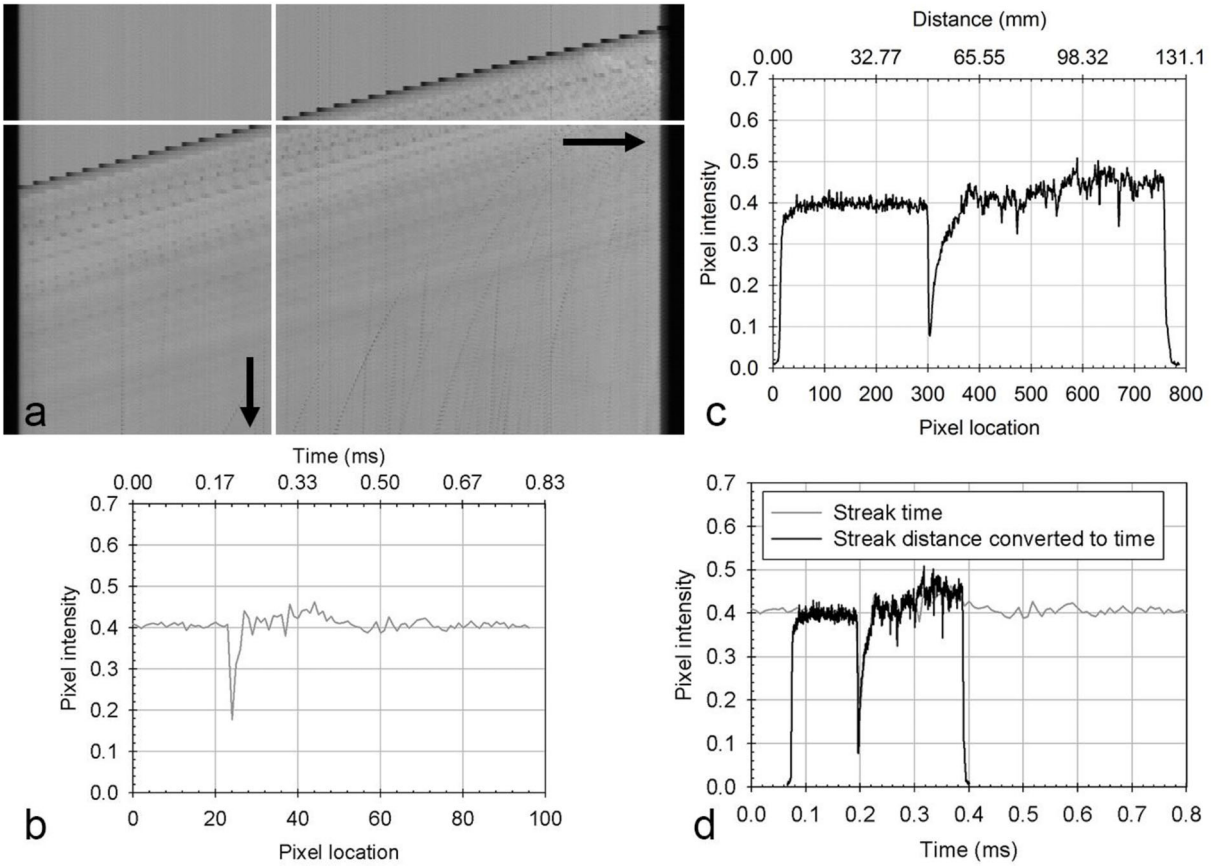

Figure 5. (a) Streak image created from the test sequence shown in Figure 4. Individual lines from the streak image are extracted to examine pixel intensity changes in the (b) vertical or time axis and (c) horizontal or distance axis. (d) The pixel intensity as a function of distance is converted to time using the shock velocity, which was measured as 387.4 $m\,s^{-1}$ (Mach 1.129).

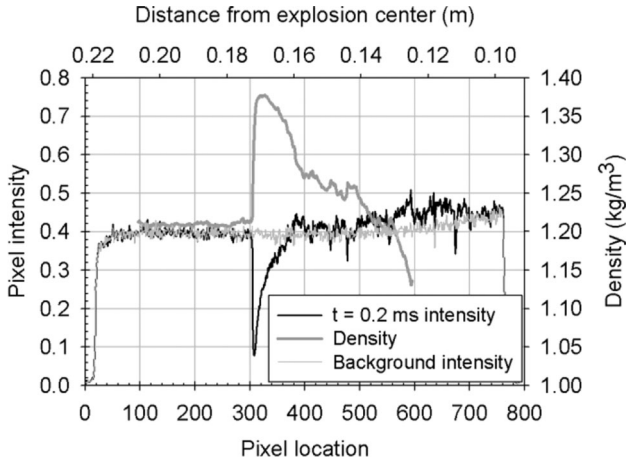

Figure 6. Graph of the measured density and intensity profiles as a function of time, calculated from the image in Figure 4d. The intensity profile is the same data as shown in Figure 5c and d.

the output density profile, at least for the large distances from the explosion center measured herein.

The temporal range of the density measurement is limited by the physical distance imaged and the velocity at which the shock wave is propagating. Several approaches were devised and attempted to lengthen the temporal measurement range by creating a "composite" schlieren image from the individual high-speed images, all of which failed. The failure is due to the nature of the schlieren imaging and Abel transform process: a full radial profile is required. Due to the spherical nature of the flow field, effects of disturbances at large radii are observed at all smaller radii, but small radial locations do not impact those further outward. In this way the leading edge of the shock wave can be imaged and quantified without imaging the explosion center, the converse however is not true. Therefore creating a composite profile is impossible because the leading shock wave is not imaged and thus its influence on smaller radial positions cannot be determined. Even attempting to temporally shift the images does not work because the shock wave and subsequent decay appearance change as the shock wave expands outward. Ultimately this limits the quantitative analysis to individual images and the achieved field of view.

In the same context, the vertical pixel intensity profile shown in Figure 5b cannot be converted directly to density because the spatial variation in pixel intensities are re-

  DOI: 10.1002/prep.201600097

quired for the Abel inversion to work. The density calculation is also limited to the regions of the image where the background intensity is uniform. Here this limits the analysis to the pixel locations between 100 and 600.

3.2 Pressure Measurement

Pressure was measured directly using a piezoelectric gage and an oscilloscope recording at 10 MHz. The pressure profiles recorded for the test shown in Figure 4, Figure 5, and Figure 6 and for a detasheet test are shown in Figure 7 and Figure 8, respectively.

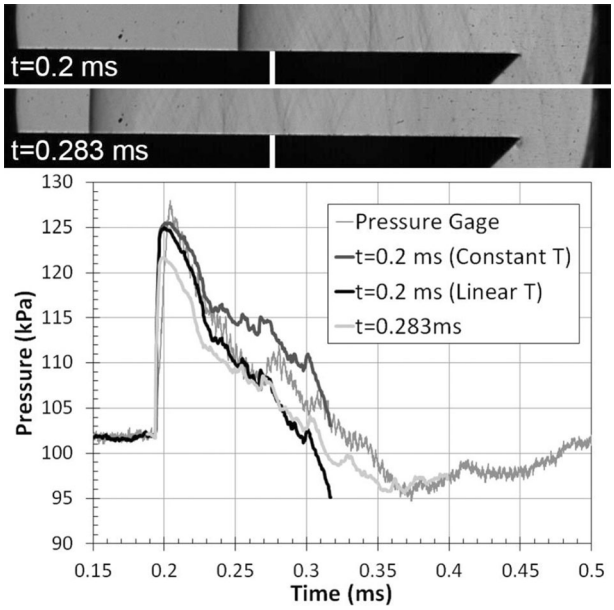

Figure 7. Calculated and measured pressure for the shotgun primer, calculated from the images shown above the plot. The top image ($t = 0.2$ ms) is the same as in Figure 4d. The pressure gage location is denoted by the vertical white line through the plate.

The optical pressures shown in Figure 7 and Figure 8 were calculated from the measured image intensity data, converted to a temporal density profile. The pressure was obtained using the ideal gas law and a temperature.

Two approaches to estimating the temperature were explored: a constant temperature and a linearly varying temperature. The constant temperature approach assumes that the passage of the shock wave increases the local gas temperature, *T*, from state 1 to 2 as a function of the shock wave Mach number, *M*, and traditional gas dynamics:

$$\frac{T_2}{T_1} = \frac{\left(1 + \frac{\gamma - 1}{2} M^2\right)\left(\frac{2\gamma}{\gamma - 1} M^2 - 1\right)}{M^2\left(\frac{2\gamma}{\gamma - 1} + \frac{\gamma - 1}{2}\right)} \tag{9}$$

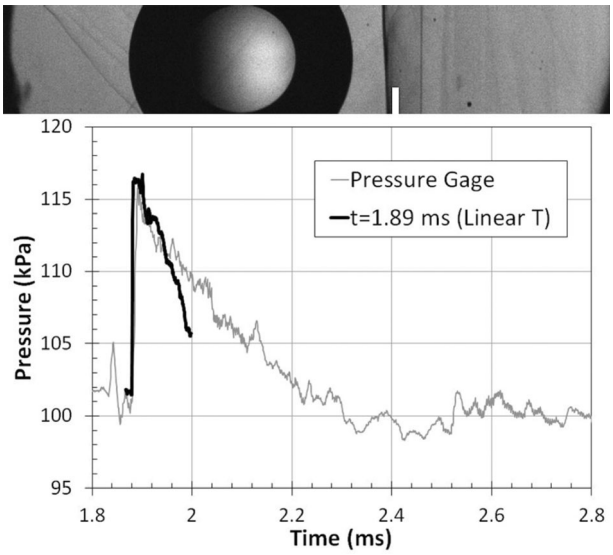

Figure 8. Calculated and measured pressure for a 1.07 g detasheet explosion. The image used for the calculation is shown above the graph. The pressure gage location is denoted by the white line on the bottom of the image behind the shock location.

where γ is the ratio of specific heats for the gas. This temperature assumption results in an over-prediction of the pressure throughout the measured blast region, because the temperature is continually decaying as the shock wave continues to expand spherically. For a Cartesian one-dimensional shock wave motion (e.g. shock tube) the constant temperature assumption would be more appropriate. This constant temperature assumption was used previously by Biss and McNesby [21].

The linear temperature variation assumes that the temperature is decaying over the same time period as the pressure and density. This assumption is essentially what is observed in the traditional Taylor similarity solution [29] and the computations shown in Figure 3. The profile is assumed here to be linear for simplicity and to not require any further assumptions on the shape of the temperature decay profile. The temperature is assumed to linearly decay from the peak temperature behind the shock wave as defined by Equation (9) to atmospheric temperature. The time at which the temperature decays to atmospheric temperature is assumed to be the same time where the density profile decays through atmospheric density. From the Taylor similarity solution [29] and computations performed, this point of decay through atmospheric conditions should occur for pressure, temperature, and density at the same time. The temperature is then assumed to remain at atmospheric temperature and not to decay further for the negative blast phase. This is again to simplify assumptions. The pressure calculated from this linear temperature decay is shown in Figure 7 and Figure 8.

The linear temperature decay assumption allows more accurate calculation of pressure from the density data than

the constant temperature assumption. The optical pressure curve closely matches the gage-measured data, including small variations. The optical data gradually diverges from the pressure gage data at increasing time values, with the optical data leading the gage data. This variation is due to the assumption of a constant shock wave velocity used to calculate the temporal density profile. A more accurate velocity profile for the shock wave would include velocity decay, which would allow the optically-measured pressure profile to more closely match the gage-measured profile. The imaging data did not have sufficient temporal and spatial resolution to estimate this decay.

Figure 7 includes measured pressure profiles from two different images. The first image is the same as shown in Figure 4d, where the shock wave is almost directly above the pressure gage. This profile accurately captures the pressure spike across the shock wave because the shock wave is located over the gage. The measurement has better temporal resolution than the pressure gage which is limited by the gage inertia. The second image is from 83 microseconds later, when the shock wave is on the left edge of the field of view. This image gives the largest data range obtained here, thus a longer measured pressure profile. This image does not capture the pressure peak as well because the shock wave has decayed, while propagating outward. The image captures the trends and small peaks in the pressure, including the negative phase and initial increase back toward atmospheric pressure. Again the poor alignment on the temporal axis is due to the constant shock wave velocity assumption, and future work will explore how to measure the velocity and velocity decay more precisely.

In Figure 8 the optical data are limited because of the presence of the lens and the shock reflection from it. The lens was in the field of view for these tests because they were conducted in the field and there were concerns that the system would not hold the calibration between tests due to the larger explosive charge and shock wave. The pressure gage fluctuation before the primary shock arrival was due to a fragment and associated oblique shock passing over the gage. The fragment is just outside the top left corner of the image in Figure 8, and the oblique shock can be observed in the top left corner of the image. The time scale in Figure 8 is referenced from the initiation of the explosive charge at time $t = 0$.

3.3 Temperature Measurement

Temperature was measured across the shock wave directly using the optically-measured density field and the pressure gage measurements, assuming ideal gas behavior. The temperature profiles for the primer and detasheet tests are shown in Figure 9 and Figure 10, respectively.

The calculated temperature for the shotgun primer in Figure 9 shows the decay from a peak temperature at the shock wave to near atmospheric temperature. The decay is over the same time-span as the gage-measured pressure decay. The data for the shock immediately over the pressure gage ($t = 0.2$ ms) agrees well with the theoretical peak temperature behind the shock wave as calculated from one-dimensional gas dynamic relationships and shock Mach number (Equation (9)). The data for the later time shows the same trend, but a higher peak, which is due to the lower density calculated behind the shock because of the decrease in the shock speed. Overall an accurate measurement of shock wave speed at the location for the measurement is critical.

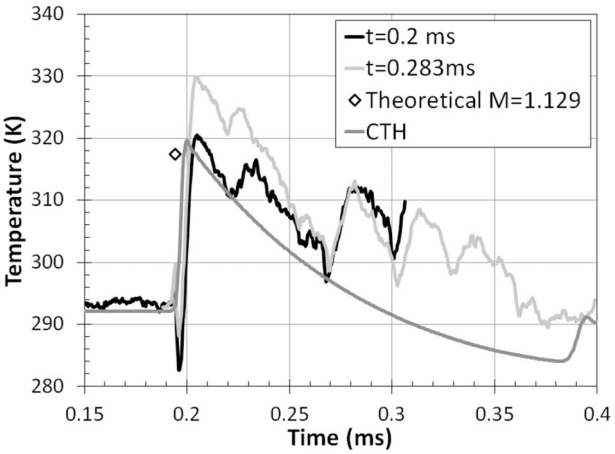

Figure 9. Temperature calculated at a distance of 0.165 m from the primer charge center.

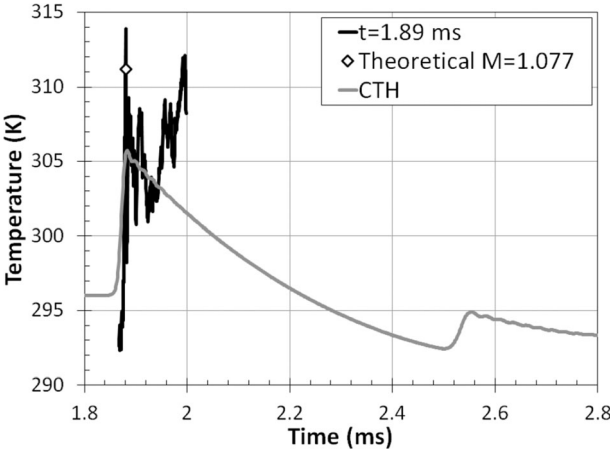

Figure 10. Temperature calculated at a distance of 0.902 m from the detasheet charge center.

The calculated temperature profile for the detasheet in Figure 10 is noisy behind the initial shock wave peak. In examining the image that the density was calculated from (in Figure 8) many weak pressure waves are visible, including an oblique shock wave near the top right hand corner. This oblique shock wave is causing the increase in temperature after about 1.9 ms. The temperature immediately behind the shock wave is still accurately determined compared to

DOI: 10.1002/prep.201600097

the one-dimensional gas dynamics calculation. The data in Figure 10 is plotted with the same axis time span as Figure 8 to highlight that the measurement is still extremely close to the shock wave position, and not much of a decay is expected in this region.

The temperature plots shown from the CTH simulations are presented herein for reference. The CTH profile for the primer was derived from the PETN simulation by scaling the output from the 1 g charge to an estimated weight of energetic material from manufacturer provided information and Sachs' scaling. The detasheet temperature was also scaled from the 1 g simulation with the known mass of PETN in the detasheet explosive charges. The scaling primarily alters the time scale of the data, so uncertainties in the explosive mass primarily results in changes to the horizontal scale of the CTH data. The profiles show reasonably good agreement with the trends for the measured data. Future work with this optical diagnostic technique could be used to develop temperature validation data for computational simulations.

The temperature measurements are overall noisy due to the combination of multiplying the density measurement with the measured pressure. Small variations in both signals are magnified in the temperature calculation. The data show the expected trend, but also show the importance of having clean experimental images and pressure traces which are free from fragments or weak pressure waves.

4 Conclusions

A technique for measuring shock wave pressures and temperatures optically was developed using quantitative schlieren imaging to measure density and simultaneous piezoelectric pressure measurements for a spherically propagating shock wave. The temperature decay behind a shock wave is measured directly from these simultaneous measurements assuming an ideal gas. The temperature measurements show that the temperature immediately behind the shock wave can be accurately estimated from one-dimensional gas dynamics relationships. The temperature profile for the shock wave from the shotgun primers exhibits a decay to atmospheric temperature over the same time period as the pressure and measured density decay, as predicted by Taylor's similarity solution [29].

Pressure measurements can be made from the optical density profile if assumptions are made regarding the temperature profile. The first assumption explored was that the peak temperature can be determined from one-dimensional gas dynamics and the shock wave Mach number. The second assumption is that the temperature decays to atmospheric temperature at the same time as the pressure and density decay to atmospheric values. Both of these assumptions were validated by the shotgun primer temperature profile, thus enabling the pressure measurement from the optical density and an assumed temperature profile.

The techniques used herein required the assumptions of a spherical shock wave propagating through a single medium and that the shock has separated from the driving product gases. Future work will explore using other reconstruction methods or multiple camera angles to allow density reconstruction in more complicated geometries. Additional work could also explore how to measure the pressure and temperature change across a gas species change, for which an accurate estimate of the ratio of specific heats and Gladstone-Dale coefficient of the gases would be required.

The technique presented herein could also be used to validate computational models for their ability to calculate temperature changes across shock waves.

Symbols and Abbreviations:

A	Abel transform matrix
B	Abel transform matrix
D	Abel transform matrix
ε	Light refraction angle
i, j	Indices
k	Gladstone-Dale constant
M	Mach number of shock wave
n	Refractive index
P	Pressure
r	Radial distance from the explosion center
T	Temperature
t	Time
x, y, z	Spatial coordinates
γ	Ratio of specific heats
δ	Non-dimensional refractive index for Abel transformation
ρ	Density

References

[1] M. Held, TNT-Equivalent, *Propellants Explos. Pyrotech.* **1983**, *8*, 158–167.
[2] P. W. Cooper, Comments on TNT Equivalence, *20th International Pyrotechnics Seminar*, Colorado Springs, CO, USA, July 25–29, **1994**, p. 215–226.
[3] P. W. Cooper, *Explosives Engineering*, Wiley-VCH, Weinheim, **1996**.
[4] R. K. Wharton, S. A. Formby, R. Merrifield, Airblast TNT Equivalence for a Range of Commercial Blasting Explosives, *J. Hazard. Mater.* **2000**, *79*, 31–39.
[5] G. S. Settles, *Schlieren and Shadowgraph Techniques: Visualizing Phenomena in Transparent Media*, Springer-Verlag, Heidelberg, **2001**.
[6] H. Kleine, J. M. Dewey, K. Ohashi, T. Mizukaki, K. Takayama, Studies of the TNT Equivalence of Silver Azide Charges, *Shock Waves* **2003**, *13*, 123–138.
[7] H. Kleine, E. Timofeev, K. Takayama, Laboratory-scale Blast Wave Phenomena-Optical Diagnostics and Applications, *Shock Waves* **2005**, *14*, 343–357.

[8] H. Kleine, H. Gronig, K. Takayama, Simultaneous Shadow, Schlieren and Interferometric Visualization of Compressible Flows, *Optics Lasers Eng.* **2006**, *44*, 170–189.
[9] M. J. Hargather, G. S. Settles, Optical Measurement and Scaling of Blasts from Gram-range Explosive Charges, *Shock Waves* **2007**, *17*, 215–223.
[10] M. M. Biss, G. S. Settles, On the Use of Composite Charges to Determine Insensitive Explosive Material Properties at the Laboratory Scale, *Propellants Explos. Pyrotech.* **2010**, *35*, 452–460.
[11] I. O. Samuelraj, G. Jagadeesh, K. Kontis, Micro-blast Waves using Detonation Transmission Tubing, *Shock Waves* **2013**, *23*, 307–316.
[12] K. L. McNesby, M. M. Biss, R. A. Benjamin, R. A. Thompson, Optical Measurement of Peak Air Shock Pressures Following Explosions, *Propellants Explos. Pyrotech.* **2014**, *39*, 59–64.
[13] J. M. Dewey, The TNT Equivalence of an Optimum Propane-oxygen Mixture, *J. Phys. D: Appl. Phys.* **2005**, *38*, 4245–4251.
[14] M. J. Hargather, Background-oriented Schlieren Diagnostics for Large-scale Explosive Testing, *Shock Waves* **2013**, *23*, 529–536.
[15] T. Mizukaki, K. Wakabayashi, T. Matsumaura, N. Nakayama, Background-oriented Schlieren with Natural Background for Quantitative Visualization of Open-air Explosions, *Shock Waves*, **2014**, *24*, 69–78.
[16] M. J. Hargather, G. S., Settles, A Comparison of Three Quantitative Schlieren Techniques, *Optics Lasers Eng.* **2012**, *50*, 8–17.
[17] A. Agrawal, B. Albers, D. Griffin, Abel Inversion of Deflectometric Measurements in Dynamic Flows, *Appl. Optics* **1999**, *38*, 3394–3398.
[18] L. Venkatakrishnan, P. Suriyanarayanan, Density Field of Supersonic Separated Flow Past an Afterbody Nozzle using Tomographic Reconstruction of BOS Data, *Experiments in Fluids* **2009**, *47*, 463–473.
[19] A. Bauknecht, B. Ewers, C. Wolf, F. Leopold, J. Yin, M. Raffel, Three-dimensional Reconstruction of Helicopter Blade-tip Vortices using a Multi-camera BOS System, *Experiments in Fluids* **2015**, *56*, 1–13.
[20] L. Venkatakrishnan, G. E. A. Meier, Density Measurements using the Background Oriented Schlieren Technique, *Experiments in Fluids* **2004**, *37*, 237–247.
[21] M. M. Biss, K. L. McNesby, *Laboratory-Scale Technique to Optically Measure Explosive Impulse for Energetic-Material Air-Blast Characterization*, Army Research Laboratory ARL-TR-6185, Adelphi, MD, USA, **2012**.
[22] L. S. Lebel, P. Brousseau, L. Erhardt, W. S. Andrews, Measurements of the Temperature Inside an Explosive Fireball, *J. Appl. Mech.* **2013**, *80*, 031702–1–6.
[23] G. Cavanough, I. Onederra, Development of Pressure and Temperature Gauges to Monitor in situ Performance of Commercial Explosives, *Mining Technol.* **2011**, *120*, 74–79.
[24] L. Smilowitz, B. Henson, M. Sandstrom, B. Asay, D. Oschwalk, J. Romero, A. Novak, Fast Internal Temperature Measurements in PBX9501 Thermal Explosions, *Shock Compress. Condens. Matter* **2005**, *845*, 1211–1214.
[25] W. K. Lewis, C. G. Rumchik, Measurement of Apparent Temperature in Post-detonation Fireballs Using Atomic Emission Spectroscopy, *J. Appl. Phys.* **2009**, *105*, 0561041–0561043.
[26] J. Densmore, B. E. Homan, M. M. Biss, K. L. McNesby, High-Speed Two-Camera Imaging Pyrometer for Mapping Fireball Temperatures, *Appl. Optics* **2011**, *50*, 2659–2665.
[27] C. J. Dasch, One-Dimensional Tomography: A Comparison of Abel, Onion-Peeling, and Filtered Backprojection Methods, *Appl. Optics* **1992**, *31*, 1146–1152.
[28] P. Kolhe, A. Agrawal, Abel Inversion of Deflectometric Data: Comparison of Accuracy and Noise Propagation of Existing Techniques, *Appl. Optics* **2009**, *48*, 3894–3902.
[29] G. I. Taylor, The Formation of a Blast Wave by a very Intense Explosion I. Theoretical Discussion, *Proc. R. Soc. London Ser. A, Mathematical Phys. Sci.* **1950**, *201*, 159–174.
[30] J. M. McGlaun, S. L. Thompson, CTH: a Three-dimensional Shock Wave Physics Code, *Int. J. Impact. Eng.* **1990**, *10*, 351–360.
[31] J. Tobin, *Quantitative Schlieren Measurement of Explosively-driven Shock Wave Density, Temperature, and Pressure Profiles*, MS Thesis, New Mexico Institute of Mining and Technology, **2014**.
[32] R. G. Gonzalez, R. E. Woods, *Digital Image Processing*, Prentice Hall, Upper Saddle River, **2008**.

Received: April 22, 2016
Revised: July 6, 2016
Published online: ■■ ■■, 0000

  DOI: 10.1002/prep.201600097

FULL PAPERS

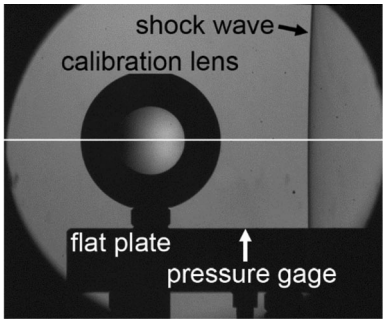

*J. D. Tobin, M. J. Hargather**

■■ – ■■

Quantitative Schlieren Measurement of Explosively-Driven Shock Wave Density, Temperature, and Pressure Profiles

DOI: 10.1002/prep.201600097 www.pep.wiley-vch.de